

Diameter-selective resonant Raman scattering in double-wall carbon nanotubesS. Bandow,¹ G. Chen,² G. U. Sumanasekera,² R. Gupta,² M. Yudasaka,³ S. Iijima,^{1,3} and P. C. Eklund^{2,*}¹*Department of Materials Science and Engineering, Japan Science and Technology Corporation, Meijo University, 1-501 Shiogamaguchi, Tenpaku, Nagoya 468-8502, Japan*²*Department of Physics, The Pennsylvania State University, University Park, Pennsylvania 16802*³*Japan Science and Technology Corporation, NEC Corporation, 34 Miyukigaoka, Tsukuba 305-8501 Japan*

(Received 30 January 2002; published 26 August 2002)

Double-wall carbon nanotubes (DWNT's) have been studied by Raman scattering using different excitation wavelengths and their spectra compared to those of single wall nanotubes (SWNT's) and C₆₀-SWNT peapods. Raman scattering from the radial and tangential vibrational modes of very small diameter $d \sim 0.6\text{--}0.9$ nm secondary (interior) semiconducting tubes within the DWNT can be unambiguously identified with 647.1 and 1064 nm excitations. The frequency of the tangential displacement vibrational modes identified with these secondary (interior) tubes is found to be downshifted by ~ 7 cm⁻¹ relative to that of the larger primary (exterior) tubes that exhibit a diameter $d \sim 1.3\text{--}1.6$ nm. This downshift strongly suggests that at small tube diameters (i.e., $d \sim 0.7$ nm), the associated wall curvature of the nanotube may require an admixture of sp^3 character in the C-C interaction. Our results also show that the value $\gamma_0 = 2.90$ eV for the nearest C-C tight binding integral is consistent with the resonant enhanced Raman scattering from DWNT's.

DOI: 10.1103/PhysRevB.66.075416

PACS number(s): 78.30.Na, 78.67.Ch

I. INTRODUCTION

Soon after the discovery of single-wall carbon nanotubes (SWNT's),¹⁻³ Raman spectroscopy was shown to provide important information regarding both the vibrational and electronic structure of these novel nanofilaments.^{4,5} The resonant nature of the Raman scattering in SWNT's was demonstrated and identified with the presence of sharp peaks (van Hove singularities) in the one-dimensional electronic density of states (DOS) of small diameter ($d < 2\text{--}3$ nm) SWNT's.^{6,7} With increasing tube diameter d , these DOS peaks decrease in separation and become more numerous, merging into a broad electronic continuum which approaches the shape of the DOS in graphene. Distinct, mirror-image pairs of these DOS peaks were later confirmed in small diameter SWNT by scanning tunneling spectroscopy,^{8,9} and the inverse relationship of the dependence of the energy spacing (E_{ii}) between these mirror image singularities on nanotube diameter (d), predicted by energy band calculations,^{10,11} was also confirmed experimentally.

The resonance in the Raman scattering cross section in SWNT's occurs when the incoming laser photon energy approximately matches a particular E_{ii} . Furthermore, the Raman-active radial breathing mode (RBM) frequency (ω_r) undergoing resonant excitation was proposed on theoretical grounds to exhibit an inverse dependence on the tube diameter d , i.e., $\omega_r \sim 1/d$, and this prediction was found consistent with the observed range of ω_r found in a given sample and correlated with that particular tube diameter distribution.⁷ Later, this simple inverse relation between RBM frequency and diameter was amended with the addition of a small constant term to take into account tube-tube interactions within a bundle of SWNT's.¹²⁻¹⁴

Recently, it has been possible to generate DWNT's by breaking the C₆₀ molecules encapsulated in SWNT's.¹⁵ Earlier Raman measurements on DWNT's was used to identify the radial breathing modes associated with both inner and

outer tubes.¹⁶ However, to the best of our knowledge, there has been no resonant Raman scattering study of DWNT's. In this paper, we present Raman results on the double wall carbon nanotubes (DWNT's) and compare them with those of SWNT's and peapods used to prepare the DWNT samples. These DWNT's are a special case of multiwall tubes (MWNT's) consisting of only two, rather than many ($\sim 3\text{--}50$), concentric seamless graphene cylinders.¹⁷ Thus, DWNT's provide an excellent new opportunity to study the Raman scattering from very small tubes. Normally, an insignificant number of these small tubes can be found in most SWNT samples prepared by arc or pulsed laser vaporization methods. We have been able to identify the Raman features associated with the smaller diameter inner tubes which are found to be as small as a $\sim(5,5)$ tube.

II. EXPERIMENT

SWNT's for this study were grown at 1200 °C in an oven by the pulsed laser vaporization of carbon target containing a $\sim 1\%$ Fe-Ni. They were subsequently purified by refluxing in HNO₃ at 160 °C. SWNT's in the liquid were centrifugally precipitated, and the liquid above the sediment was decanted. Neutral SWNT's were obtained by adding distilled water to the sediment and repeating the centrifugal precipitation several times. After drying, the SWNT's were subjected to heat treatment in dry air (420 °C, 20 min.) in order to remove residual amorphous carbon attached on the walls of the SWNT's. It was also found that this process was essential for opening the tube ends.¹⁸

DWNT's were prepared from these purified and opened SWNT's. As a first step, "peapod" structures were prepared by introducing chains of closepacked C₆₀ molecules inside the preexisting SWNT's that exhibited a most probable diameter in the range $\sim 1.3\text{--}1.4$ nm. This was accomplished by the diffusion of C₆₀ molecules inside the tubes from the C₆₀ vapor maintained at 400 °C in a sealed and evacuated

glass ampoule.¹⁸ The DWNT's were subsequently derived from the peapods by heating them at 1200 °C in vacuum ($<10^{-6}$ Torr). Such a high-temperature heat treatment was found previously to induce the coalescence between C_{60} molecules, resulting in the growth of a secondary tube inside the primary tube.¹⁶ Typical high-resolution transmission electron microscopy images of the peapod structures and the DWNT's have been published previously.^{19,20} The unbroken lengths of the inner tube are quite long, typically exceeding several hundred nm. The samples used for the Raman studies were characterized using transmission electron microscopy.

Raman scattering was excited in the visible using a mixed gas Ar-Kr ion laser giving output at 488.0 nm (2.54 eV), 514.5 nm (2.41 eV), 647.1 nm (1.92 eV), and in infrared at 1064 nm (1.17 eV) with a Nd:YAG laser. The Raman spectra with visible excitation energies reported here were measured using a Jobin Yvon HR460 single-grating monochromator equipped with a liquid nitrogen cooled charge-coupled array detector and a holographic notch filter (Kaiser Optical Systems, Inc., Ann Arbor, MI, USA). The sample was in the form of a loosely compacted pellet. To avoid laser damage to the sample, all the visible Raman data were taken at low laser power density ($\sim 2 \text{ W cm}^{-2}$) focusing the radiation to a $\sim 0.1 \text{ mm} \times 1 \text{ mm}$ stripe with a cylindrical lens. The laser was incident at 45° to the substrate and scattered light collected in back scattering to minimize stray light. No polarization analyzer was used, hence both perpendicular and parallel polarized light were collected. For accurate determination of Raman peak positions, lines from several atomic spectral lamps (Hg and Ar) were used for spectral calibration. The Nd-YAG-excited Raman spectra were collected at room temperature in the true backscattering geometry using a FT-Raman spectrometer (BOMEM DA3+).

III. RESULTS

A. Radial breathing mode region

The Raman scattering spectra in the low frequency region ($80\text{--}400 \text{ cm}^{-1}$) taken with 488.0, 514.5, 647.1, and 1064 nm excitations are shown in the four panels of Fig. 1. In all the panels, the top, middle, and bottom spectra refer, respectively, to DWNT's, peapods, and primary SWNT's. A remarkable difference in the spectra between 250 and 400 cm^{-1} can be observed for all excitation wavelengths except 488 nm. In this frequency range, only very weak, or no Raman features are observed for both SWNT's and peapods, yet the DWNT sample exhibits several new peaks. Below 250 cm^{-1} , the line shape of the strongest band observed near $\sim 160 \text{ cm}^{-1}$ shows some sensitivity to the excitation wavelength. However, the shape of these lower frequency bands is essentially independent of whether we consider the response of peapods, DWNT's, or SWNT's. This indicates two main points: (1) The bands should be identified with the vibrational features of the primary (outer) tubes and (2) these primary tube Raman features are not strongly influenced by the presence of either the fullerenes ("peas") or secondary tubes inside these primary tubes. Of course, we can reach this conclusion only because the three samples are all derived from the same SWNT material.

It is clear from Fig. 1 that the Raman bands detected in the frequency range between ~ 250 and $\sim 400 \text{ cm}^{-1}$ for DWNT's must be associated with the radial breathing modes of the secondary (or inner) tubes.¹⁶ Theoretical calculations have been put forward for the diameter dependence of the radial breathing mode frequency (ω_r) for an isolated single-walled carbon nanotubes. Various methods have been used and there is general agreement that the result does not depend significantly on the chirality (only the tube diameter d). Furthermore, the functional form is found to be $d = A/\omega_r$, where A is a constant, ω_r the RBM frequency, and d is the tube diameter. The following values of A have been reported: $223 \text{ cm}^{-1} \text{ nm}$ (zone folding method⁵), $218 \text{ cm}^{-1} \text{ nm}$ (force constant model²¹), $234 \text{ cm}^{-1} \text{ nm}$ (local density approximation²²), $236 \text{ cm}^{-1} \text{ nm}$ (pseudopotential density functional theory,²³ $227 \text{ cm}^{-1} \text{ nm}$ (elastic deformation model²⁴). It should be noted that the elastic deformation calculation of Mahan²⁴ determines an analytical formula for the RBM frequency that depends only on the diameter and the values of the transverse and longitudinal in-plane sound velocities of graphite. On the other hand, the theory does not take into account the small effects of the tube wall curvature. The effect of tube-tube interactions on the breathing mode have also been considered, and for a tube with diameter close to that of a (10,10) tube, the correction due to bundling is²⁵ $\sim 14 \text{ cm}^{-1}$ or slightly higher¹⁴ $\sim 22 \text{ cm}^{-1}$. A series of experiments by Dresselhaus and co-workers on isolated tubes lying on a SiO_2/Si substrate arrive at a value of $A = 248 \text{ cm}^{-1} \text{ nm}$;²⁶ this value for A includes a small, but unknown, contribution from the tube-substrate interaction. It should be recognized that the present samples are in the form of bundles of DWNT. Therefore, there are two tube-tube interactions that can shift slightly the effective value of the radial breathing mode: outer tube-outer tube interactions and outer tube-inner-tube interactions. The latter has not been calculated. To analyze the RBM data for our DWNT samples, we adopt a simple view. We neglect the small effect of the tube-tube interactions and simply take the mean value for A from all the work cited above, i.e., $A = 234 \text{ cm}^{-1} \text{ nm}$. If, instead we were to have chosen the lowest and highest value of A , there would be only a $\sim \pm 5\%$ change in A and therefore a 5% uncertainty in diameter values calculated from the observed DWNT RBM frequencies. The results for d using this relation are summarized in Table I. From the table, the RBM frequencies imply that the diameters for primary tubes are roughly in the range of $\sim 1.3\text{--}1.6 \text{ nm}$, and those for the inner (secondary) tubes in DWNT's are considerably smaller, as expected, and in the range of $\sim 0.6\text{--}0.9 \text{ nm}$. The difference in the mean diameter of the external (primary) and internal (secondary) tube $\Delta \bar{d} = \bar{d}_{\text{ext}} - \bar{d}_{\text{int}} \approx 0.7 \text{ nm}$. This value for $\Delta \bar{d}$ is consistent with the π -electron cloud thickness ($t \sim 0.34 \text{ nm}$), suggesting that the inner tubes are tightly nested inside the primary (external) tube.

B. Tangential mode region

The Raman scattering from the tangential carbon atom vibrations (T band) is normally detected at $\sim 1592 \text{ cm}^{-1}$ for typical SWNT's with $d \sim 1.4 \text{ nm}$. The line shape of this

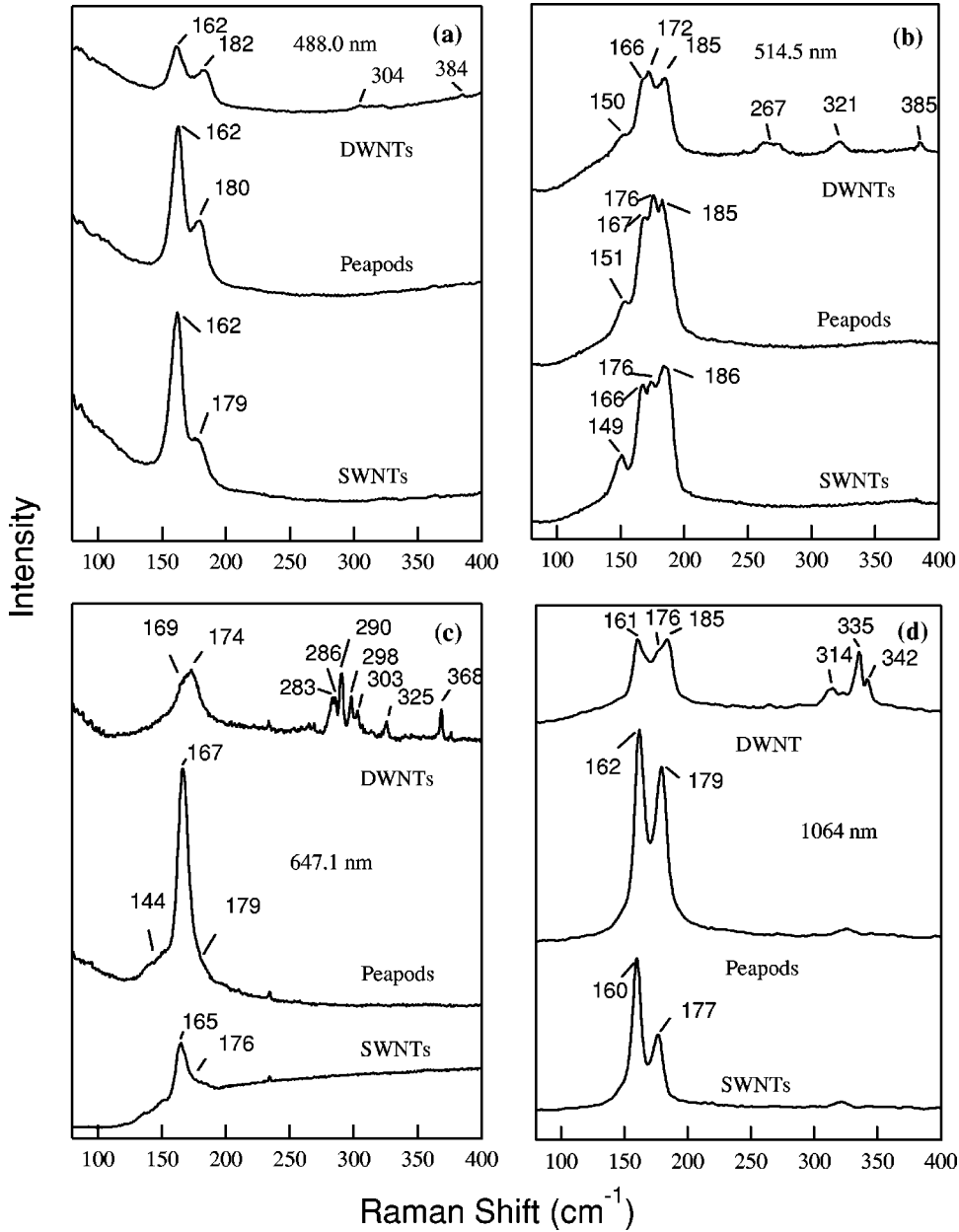


FIG. 1. Radial breathing mode Raman spectra for SWNT's, DWNT's, and C_{60} -SWNT peapods using different excitation energies of 488.0 (a), 514.5 (b), 647.1 (c), and 1064(d) nm. The spectra were fitted to an appropriate sum of Lorentzians and the obtained peak positions are marked on the respective spectra.

band depends on the excitation laser energy,⁵ and has been shown to exhibit a broad band when excited in the red (~ 1.9 eV or 647.1 nm), and narrower features for other typical excitation frequencies such as 488 nm (2.55 eV) and 514 nm (2.42 eV). The broad T -band excited at ~ 1.9 eV has been identified with scattering from metallic tubes, and the narrower T bands with semiconducting tubes.⁵ The metallic tube Raman scattering resonates at ~ 2 eV because this is the spacing between the first pair of van Hove singularities in metallic tubes in this diameter range. The line broadening of the Raman band has been assigned to Fano resonance arising due to electron-phonon coupling.²⁷

The Lorentzian (L) and Breit Wigner Fano (BWF) Raman line shape functions are given by

$$L(\omega) = \frac{I_0 \Gamma}{(\omega - \omega_0)^2 + \Gamma^2}, \quad (1)$$

$$\text{BWF}(\omega) = I'_0 \frac{\left(1 + \frac{\omega - \omega_0}{q\Gamma}\right)^2}{1 + \left(\frac{\omega - \omega_0}{\Gamma}\right)^2}, \quad (2)$$

where ω_0 and Γ are the peak position and half width at full maxima for the Lorentzian line shape function. The asymmetry of the BWF function depends on a coupling parameter ($1/q$) which is a measure of the strength of the interaction between the phonon and the conduction electrons (in metallic tubes). In the limit $1/q \rightarrow 0$ the BWF function becomes a Lorentzian. In this context, we expect a Lorentzian line shape when the electron-phonon coupling is small (semiconducting SWNT's) and a BWF line shape when $1/q$ is large (metallic tubes).

In Fig. 2, we show the Raman spectra in the high-

TABLE I. Tube diameters estimated from radial breathing mode (RBM) frequencies. The tube diameters were calculated from $d=234/\omega_r$ (as explained in the text), where d is the tube diameter (nm) and ω_r , the RBM frequency (cm^{-1}). The data with * and † are for peapods and SWNT's, respectively. The data for DWNT's are indicated without mark. The diameters for primary tubes are in the range of $\sim 1.3\text{--}1.6$ nm, and for secondary tubes in DWNT's of $\sim 0.6\text{--}0.9$ nm.

Excitation	Primary tubes		Secondary tubes		Excitation	Primary tubes		Secondary tubes	
	ω_r	d	ω_r	d		ω_r	d	ω_r	d
488 nm	162	1.44	304	0.77	514 nm	150	1.56	267	0.88
	182	1.29	384	0.61		166	1.41	321	0.73
						172	1.36	385	0.61
						185	1.26		
	162*	1.44*				151*	1.55*		
	180*	1.30*				167*	1.40*		
						176*	1.33*		
						185*	1.26*		
	162†	1.44†				149†	1.57†		
	179†	1.31†				166†	1.41†		
						176†	1.33†		
						186†	1.26†		
647 nm	169	1.38	283	0.83	1064 nm	161	1.45	314	0.75
	174	1.34	286	0.82		176	1.33	335	0.70
			290	0.81		185	1.26	342	0.68
			298	0.78					
			303	0.77					
			325	0.72					
			368	0.64					
	144*	1.62*				162*	1.44*		
	179*	1.31*				179*	1.31*		
	165†	1.42†				160†	1.46†		
	176†	1.33†				177†	1.32†		

frequency region $1450\text{--}1650\text{ cm}^{-1}$ that contain the SWNT T bands. The four panels refer to the excitation wavelengths (488, 514.5, 647.1, and 1064 nm). In each panel the DWNT peapod and primary SWNT spectra appear on top, middle, and bottom, respectively. Our experimental results for SWNT (Fig. 2) are also in agreement with the previously reported results, as evidenced by the broad tangential bands observed with 647.1 nm excitation and narrow tangential bands detected with 488, 514.5, and 1064 nm excitation. In the latter (semiconducting) case, the T -band line shape is well represented by the superposition of Lorentzian components of semiconducting tube modes. On the other hand, the Raman spectra acquired with 647.1 nm excitation are well fit by the superposition of two different line shapes: several symmetric Lorentzian components and an asymmetric Breit-Wigner-Fano component.²⁷ The fits of Lorentzian and BWF line shapes to the data are shown in Fig. 2 as the sum of the contributions (dotted line) and the individual contributions (dash-dotted line). It should be recalled that the BWF peak position is close to the renormalized phonon frequency ($\bar{\omega}$) (renormalized via the coupling of the phonon to the electronic states), and not the discrete (uncoupled) phonon mode ($\bar{\omega}$). In Fig. 2, the renormalized and uncoupled phonon frequencies⁵ are indicated inside and without parentheses,

respectively. The details of the analysis of these components are described in the next section.

IV. DISCUSSION

Due to the one-dimensional nature of the SWNT, the electronic density of states (DOS) exhibits pairs of van Hove singularities located approximately equidistant above and below the Fermi energy.²⁸ In a tight binding energy band model, the energy separation of these DOS singularities can be connected with tube diameter d via the nearest-neighbor C-C tight binding integral γ_0 . The pioneering work for calculating the energy separations between mirror-image DOS singularities (E_{ii}) as a function of d was carried out by Kataura *et al.*¹⁰ and is shown in Fig. 3 as a plot of E_{ii} vs $1/d$. It is evident that this inverse relationship between E_{ii} and d is almost linear. Each point in the Kataura plot represents the calculation for a particular symmetry (n, m) tube. The dark and open symbols respectively, represent metallic and semiconducting tubes. The lowest three sets of data are particularly useful because they are well separated from the other higher E_{ii} data. E_{11}^S , E_{22}^S , and E_{11}^M refer to the spacing between singularities in a semiconducting (s) and metallic (m) tubes; the subscript ii ($i=1,2$) refer to the lowest ($i=1$) and

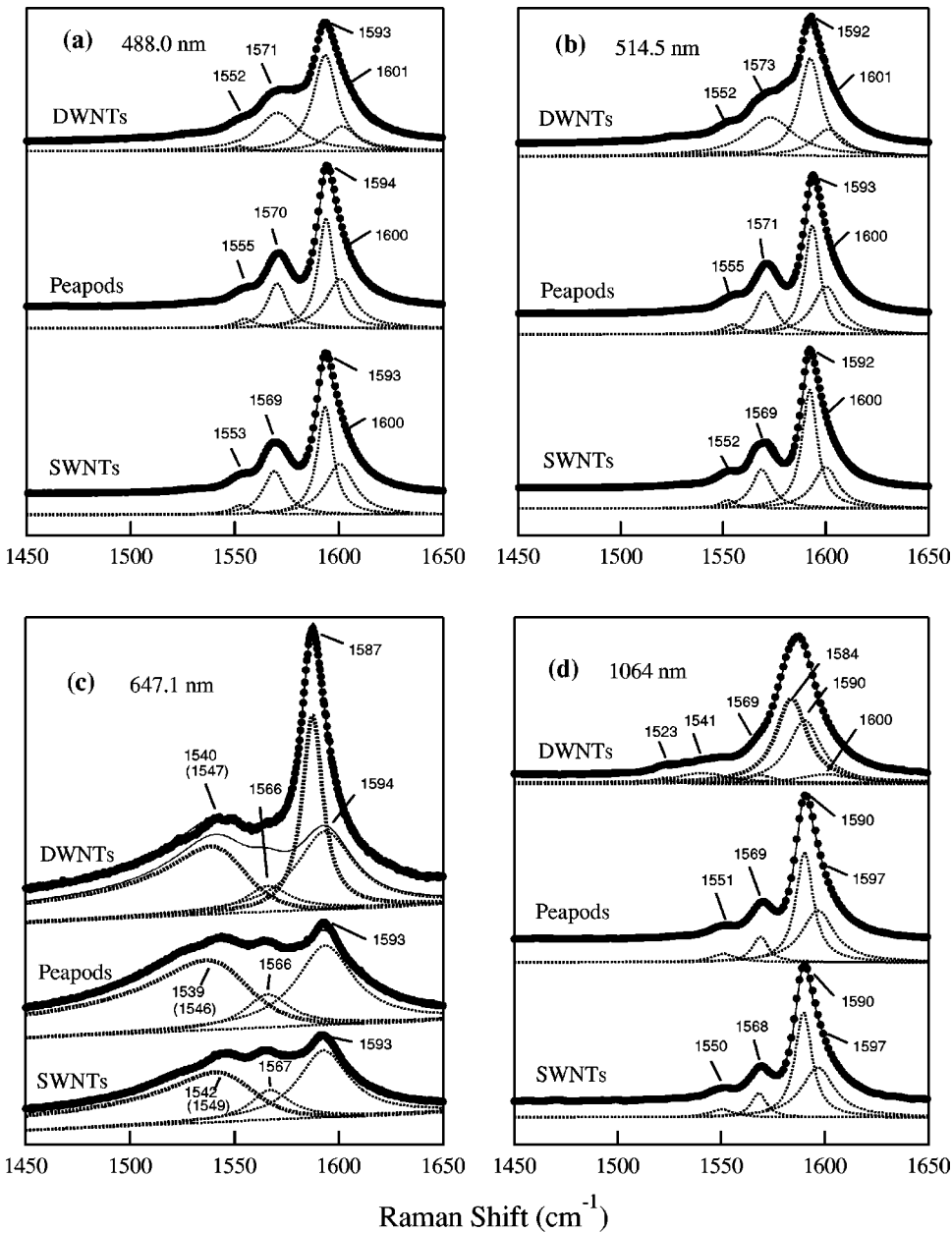


FIG. 2. Raman scattering spectra for the tangential mode region. The excitation energies are indicated in each panel. Lorentzian components associated with the primary semiconducting tubes are indicated by the thin dotted lines, and those with the secondary tubes in DWNT's are indicated by the thick dotted lines in (c) and (d) (see text). The asymmetric Breit-Wigner-Fano (BWF) component is also represented by the thick dotted line in (c) and (d), where the coupling parameter ($1/q$) between the discrete phonon mode and continuum modes, determining the asymmetry of the line shape, was fixed at -0.35 [from Rao *et al.* (Ref. 27)]. The numerical values in the parentheses are the renormalized phonon frequencies of the BWF lines (see text). The thin solid line in (c) is a sum of thin dotted Lorentzian components and the BWF component, which is similar to the spectra taken for SWNT's and peapods.

next highest ($i=2$) separation between filled valence bands and empty conduction bands. The results of these calculations are very helpful to explain the experimental results of resonant Raman scattering in SWNT's. The resonance occurs for a particular diameter tube when the laser energy matches the separation between a particular pair of mirror image DOS singularities. Figure 3 shows the diameter dependence of E_{ii} using the value for $\gamma_0=2.90$ eV (based on Ref. 10), where E_{ii} for the metallic tubes are indicated by the solid circles, and E_{ii} for the semiconducting tubes by the open circles. From the pattern of symbols in the figure, it is easy to see that a simple $1/d$ relationship exists between the tube diameter and E_{ii} for the three lowest pairs of mirror image DOS spikes. As the energy spacing E_{ii} increases with decreasing d , the chirality (n,m) of the tubes spreads the results of E_{ii} vs $1/d$ into bands of results. Eventually these bands merge into a continuum (Fig. 3). We can use the RBM frequencies

to estimate the range of d values for our samples (see Table I). There must be two ranges when we consider DWNT's. The ranges for the primary (outer) and secondary (inner) tubes are indicated by the region between thick vertical bars of Fig. 3. Horizontal lines in Fig. 3 indicate the laser photon energies which we have used to excite the resonant scattering.

As can be seen from Fig. 3, 488 and 514.5 nm excitation energies match well with the third largest E_{ii} spacing of the primary semiconducting tubes E_{33}^S (open circles located just above the solid circles). Therefore, for these excitations, resonant Raman scattering from primary semiconducting tubes should occur. On the other hand, for secondary tubes, 488 and 514.5 nm excitations are seen to be unsuitable for resonant enhancement; only the smaller secondary tubes ($d \sim 0.7$ nm) inside the DWNT's are likely to exhibit resonant Raman scattering for 514.5 nm excitation via the second- E_{ii}

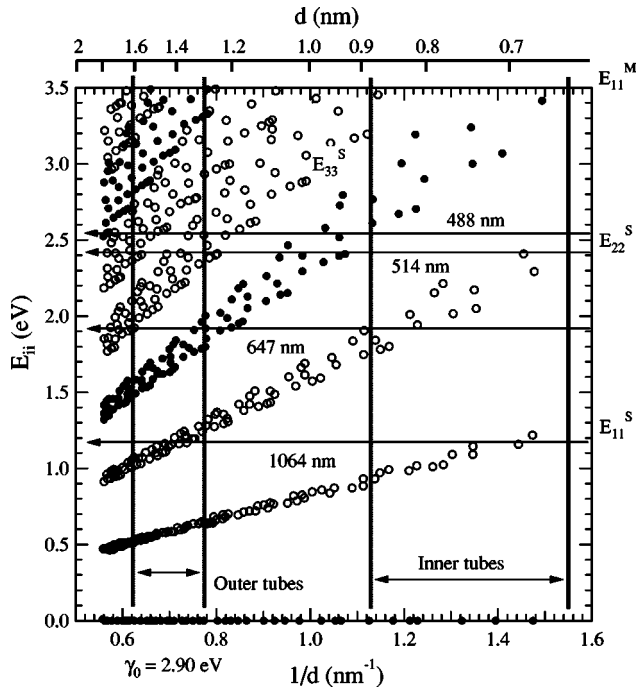


FIG. 3. Tube diameter (d) dependence of the energy separation [E_{ii}^x , $x=s$ (semiconductor), or $x=m$ (metal)] between mirror-image spikes of van Hove singularities. The solid circles are for metallic tubes and the open circles are for semiconducting tubes. All data points are based on the work of Kataura *et al.* (Ref. 10), but here we set the tight binding integral, $\gamma_0 = 2.90$ eV. The primary (external) and secondary (internal) tube diameters existing in the samples occupy the region between the thick vertical lines.

branch for semiconducting tubes (E_{22}^S). Therefore, the Raman scattering spectra recorded for the RBM bands [Figs. 1(a) (488 nm) and 1(b) (514.5 nm)] and tangential mode [Figs. 2(a) (488 nm) and 2(b) (514.5 nm)] vibrations are expected to be quite similar. The new features in the range 250–400 cm^{-1} are therefore identified with new RBM bands associated with the smaller diameter secondary tubes produced by the peapod coalescence.

The T bands in DWNT are found to be slightly broadened relative to the SWNT T bands. It is worth noting here that the RBM features associated with the primary tubes are not modified significantly by the presence of fullerenes (peapods) and internal tubes (DWNT's), indicating a small interaction between the host tubes and these "dopants." This further indicates that only a very small charge transfer could take place with the primary tube and the C_{60} or interior tube. Alkali metal or bromine doping of the SWNT's significantly modifies the vibration features of SWNT's due to the electron charge transfer from dopants to SWNT's (for K and Rb) and vice versa (for Br_2).²⁷ Apparently, the charge transfer between tubes in a MWNT, or in this case, the DWNT is not strong enough to be easily observed by Raman scattering. Intense tangential bands observed with 488 nm, 514.5 nm and 1064 nm excitation are all detected with peak positions near 1593 cm^{-1} with satellite peaks located at lower frequencies. They are most probably associated with the primary semiconducting tubes, and the satellite peaks at lower

frequencies are identified by the zone folding of the phonon dispersion of a graphene sheet due to the cyclic boundary condition of the SWNT.²⁹

In the case of 647.1 nm excitation, the Raman scattering from the primary (larger diameter) metallic tubes should be enhanced due to resonant scattering involving E_{11}^M (solid circles, see Fig. 3). In addition, the largest secondary semiconducting tubes in DWNT's should exhibit resonant Raman scattering using E_{22}^S . This is the origin of the new intense RBM band at ~ 290 cm^{-1} in Fig. 1(c) that is identified with the secondary (inner) tubes in the DWNT's corresponding to $d \sim 0.8$ nm (see Table I). Also for 647.1 nm excitation, the Raman-active tangential mode band for SWNT's and peapods can be well represented by the superposition of two Lorentzian lines [thin dotted lines in Fig. 2(c)] and one BWF line (thick dotted line). The latter BWF line should be associated with the primary metallic tubes. The renormalized phonon frequencies of the BWF lines [1541 cm^{-1} (peapods), 1547 cm^{-1} (DWNT's), and 1546 cm^{-1} (SWNT's)] are significantly downshifted relative to the most intense Lorentzian T band associated with the primary semiconducting tubes (~ 1593 cm^{-1}). It is interesting that this renormalized frequency is significantly lower (~ 5 cm^{-1}) for the peapod sample. Perhaps, this signals a weak charge transfer between the C_{60} molecules and the nanotube. Using 647.1 nm excitation, there is significant intensity in a Lorentzian line at ~ 1593 cm^{-1} for all three samples. Thus, it should be associated with the primary tubes. However, according to Fig. 3 only very large primary semiconducting tubes can fit the scheme of Fig. 3 via E_{33}^S .

For DWNT's with 647.1 nm excitation, a new Lorentzian component can be observed as indicated by the thick dotted line centered at 1587 cm^{-1} in Fig. 2(c), together with the contribution from the primary tubes (thin solid line; sum of two Lorentzians and one BWF line). From Fig. 3, a ~ 0.8 nm diameter secondary semiconducting tube should exhibit resonant Raman scattering via E_{22}^S . Therefore, the new T -band peak detected for DWNT's might be associated with small secondary semiconducting tubes with $d \sim 0.8$ nm. The vibrational frequency of this smaller diameter tube is ~ 7 cm^{-1} less than that of the larger diameter semiconducting tubes. This observation is consistent with the results of the spectral analysis of the 1064 nm excited Raman spectrum, as described next. It is important to note that the diameter dependence of the T band is expected on theoretical grounds to be very weak for sp^2 bonded SWNT's. An experimental observation of this weak dependence has not been reported to date. We propose that at these small diameters, the admixture of sp^3 character into the C-C interactions might explain this 7 cm^{-1} shift.

From the RBM band detected at around 335 cm^{-1} for DWNT's with 1064 nm excitation [see Fig. 1(d) and Fig. 3 for $\gamma_0 = 2.90$ eV], we can say that the resonant Raman scattering from ~ 0.7 nm diameter secondary tubes (see Table I) is taking place. A new Lorentzian component at 1584 cm^{-1} , as shown in Fig. 2(d) by the thick dotted line is observed. Since the resonant enhancement of the Raman scattering at 1064 nm excitation is identified with secondary

semiconducting tubes, the peak at 1584 cm^{-1} can be attributed to the secondary semiconducting tubes with $d \sim 0.7\text{ nm}$. The peak position of this transverse phonon peak from the secondary tubes is also downshifted by $\sim 7\text{ cm}^{-1}$ as compared with that from the primary tubes. This is further evidence that the T bands for smaller diameter tubes exhibit a tendency to downshift slightly (perhaps due to wall curvature).

Finally, we discuss about the appropriateness of the value $\gamma_0 = 2.90\text{ eV}$ used in the present analysis. According to the analysis of previous optical absorption spectra,^{10,30} the value $\gamma_0 = 2.75\text{ eV}$ was obtained after consideration of a possible exciton effect which upshifts the lowest optical interband transition energy (first- E_{11}) of semiconducting tubes due to the additional transition to the excitonic band. However, this exciton effect should be absent in the metallic tubes. As a consequence, the exciton transition only modifies E_{11}^S , and increases the optical absorption peak by only $\sim 0.08\text{ eV}$ for $d \sim 1.3\text{ nm}$ tubes.³⁰ If we take into account the proposed exciton effect, the values for E_{11}^S is perhaps upshifted by $\sim 10\%$. Even after correcting for this effect, the modification of the resonant condition appears only a small effect in the secondary tubes studied with 1064 nm excitation. Therefore, it does not have much impact on the results presented here. In addition, it should be noted that it is necessary to use $\gamma_0 = 2.90\text{ eV}$ in order to explain the resonant enhancement of Raman scattering from metallic tubes by 647.1 nm excitation.

In summary, the room temperature Raman scattering spectrum for SWNT's, peapods and DWNT's using 488 , 514.5 , 647.1 , and 1064 nm excitation energies was obtained. The RBM Raman scattering gives important information

about the tube diameters present in the samples and about the resonant enhancement of the Raman scattering from the selected tubes. From the analysis of Raman spectra using Fig. 3 and tube diameters inferred from the RBM frequencies, the tangential mode frequencies of the primary semiconducting tubes ($\sim 1.3\text{--}1.6\text{ nm}$ diameter) and the secondary semiconducting tubes in DWNT's ($\sim 0.6\text{--}0.9\text{ nm}$ diameter) can be separated, respectively, into $\sim 1590\text{--}1594\text{ cm}^{-1}$ and $\sim 1584\text{--}1587\text{ cm}^{-1}$. In addition, the primary metallic tubes with $d \sim 1.3\text{--}1.6\text{ nm}$ gave asymmetric BWF type Raman scattering lines with 647.1 nm excitation. The renormalized phonon frequencies of these BWF lines are in the range of $1541\text{--}1547\text{ cm}^{-1}$, which are considerably smaller than the phonon frequencies of semiconducting tubes ($\sim 1590\text{--}1594\text{ cm}^{-1}$). This downshift has been explained by the effect of screening the C-C interaction due to the conduction electrons of metallic tube. The nearest C-C tight binding integral $\gamma_0 = 2.90\text{ eV}$ was applied to explain the experimental results.

ACKNOWLEDGMENTS

This work is supported, in part, by the Japanese Ministry of Education, Science, Sports and Culture (Grant-in-Aid for Scientific Research on the Priority Areas Fullerenes and Nanotubes) and by Meijo University (S.B). We also gratefully acknowledge the Japan Society for the Promotion Science (S.B.) and the National Science Foundation (P.C.E), Grant No. INT-9815744, for travel funds to exchange researchers between Japan and the United States. G.C. was supported by the Penn State NSF MRSEC program. R.G. was supported by the University of Pennsylvania-MRSEC program.

*Author to whom correspondence should be addressed; Email address: pce3@psu.edu

¹S. Iijima and T. Ichihashi, *Nature (London)* **363**, 603 (1993).

²D. S. Bethune, C. H. Kiang, M. S. de Vries, G. Gorman, R. Savoy, J. Vazquez, and R. Beyers, *Nature (London)* **363**, 605 (1993).

³Y. Saito, T. Yoshikawa, M. Okuda, N. Fujimoto, K. Sumiyama, K. Suzuki, A. Kasuya, and Y. Nishina, *J. Phys. Chem. Solids* **54**, 1849 (1993).

⁴J. M. Holden, P. Zhou, X.-X. Bi, P. C. Eklund, S. Bandow, R. A. Jishi, K. D. Chowdhury, G. Dresselhaus, and M. S. Dresselhaus, *Chem. Phys. Lett.* **220**, 186 (1994).

⁵A. M. Rao, E. Richter, S. Bandow, B. Chase, P. C. Eklund, K. A. Williams, S. Fang, K. R. Subbaswamy, M. Menon, A. Thess, R. E. Smalley, G. Dresselhaus, and M. S. Dresselhaus, *Science* **275**, 187 (1997).

⁶R. Saito, T. Takeya, T. Kimura, G. Dresselhaus, and M. S. Dresselhaus, *Phys. Rev. B* **57**, 4145 (1998).

⁷S. Bandow, S. Asaka, Y. Saito, A. M. Rao, L. Grigorian, E. Richter, and P. C. Eklund, *Phys. Rev. Lett.* **80**, 3779 (1998).

⁸J. W. G. Wildoer, L. C. Venema, A. G. Rinzier, R. E. Smalley, and C. Dekker, *Nature (London)* **391**, 59 (1998).

⁹T. W. Odom, J.-L. Huang, P. Kim, and C. M. Lieber, *Nature (London)* **391**, 62 (1998).

¹⁰H. Kataura, Y. Kumazawa, Y. Maniwa, I. Umez, S. Suzuki, Y. Ohtsuka, and Y. Achiba, *Synth. Met.* **103**, 2555 (1999).

¹¹R. Saito, G. Dresselhaus, and M. S. Dresselhaus, *Phys. Rev. B* **61**, 2981 (2000).

¹²M. S. Dresselhaus and P. C. Eklund, *Adv. Phys.* **49**, 705 (2000).

¹³J. Kürti, H. Kuzmany, B. Burger, M. Hulman, J. Winter, and G. Kresse, *Synth. Met.* **103**, 2508 (1999).

¹⁴L. Henrard, E. Hernandez, P. Bernier, and A. Rubio, *Phys. Rev. B* **60**, R8521 (1999).

¹⁵D. E. Luzzi and B. W. Smith, in *Science and Application of Nanotubes*, edited by D. Tomañek and R. J. Enbody (Kluwer, New York, 2000), p. 67.

¹⁶S. Bandow, M. Takizawa, K. Hirahara, M. Yudasaka, and S. Iijima, *Chem. Phys. Lett.* **337**, 48 (2001).

¹⁷For general reviews see M. S. Dresselhaus, G. Dresselhaus, and P. C. Eklund, *Science of Fullerenes and Carbon Nanotubes* (Academic Press, New York, 1996); R. Saito, G. Dresselhaus, and M. S. Dresselhaus, *Physical Properties of Carbon Nanotubes* (Imperial College Press, London, 1998).

¹⁸K. Hirahara, K. Suenaga, S. Bandow, H. Kato, T. Okazaki, H. Shinohara, and S. Iijima, *Phys. Rev. Lett.* **85**, 5384 (2000).

¹⁹B. W. Smith, M. Monthieux, and D. E. Luzzi, *Nature (London)* **396**, 323 (1998).

²⁰B. W. Smith and D. E. Luzzi, *Chem. Phys. Lett.* **321**, 169 (2000).

- ²¹R. A. Jishi, L. Venkataraman, M. S. Dresselhaus, and G. Dresselhaus, *Chem. Phys. Lett.* **209**, 77 (1993).
- ²²J. Kürti, G. Kresse, and H. Kuzmany, *Phys. Rev. B* **58**, R8869 (1998).
- ²³D. Sánchez-Portal, E. Artacho, J. M. Soler, A. Rubio, and P. Ordejón, *Phys. Rev. B* **59**, 12 678 (1999).
- ²⁴G. D. Mahan, *Phys. Rev. B* **65**, 235402 (2002).
- ²⁵U. D. Venkateswaran *et al.*, *Phys. Rev. B* **59**, 10 928 (1999).
- ²⁶M. S. Dresselhaus, G. Dresselhaus, A. Jorio, A. G. S. Filho, and R. Saito, *Carbon* (to be published).
- ²⁷A. M. Rao, P. C. Eklund, S. Bandow, A. Thess, and R. E. Smalley, *Nature (London)* **388**, 257 (1997).
- ²⁸R. Saito, M. Fujita, G. Dresselhaus, and M. S. Dresselhaus, *Appl. Phys. Lett.* **60**, 2204 (1992).
- ²⁹A. Kasuya, Y. Sasaki, Y. Saito, K. Tohji, and Y. Nishina, *Phys. Rev. Lett.* **78**, 4434 (1997).
- ³⁰M. Ichida, S. Mizuno, Y. Tani, Y. Saito, and A. Nakamura, *J. Phys. Soc. Jpn.* **68**, 3131 (1999).